Implementation of a new Cryopad on the diffractometer POLI at MLZ

V. Hutanu^{1,2}, W. Luberstetter^{1,2}, E. Bourgeat-Lami³, M. Meven^{1,2}, A. Sazonov^{1,2}, A. Steffen² G. Heger¹, G. Roth¹, E. Lelièvre-Berna³

¹ Institut für Kristallographie RWTH Aachen University, Jägerstr. 17-19, 52056 Aachen Germany
² Jülich Centre for Neutron Science (JCNS) at Heinz Maier-Leibnitz Zentrum (MLZ),
Forschungszentrum Jülich GmbH, Lichtenbergstr. 1, 85747 Garching, Germany
³ Institut Laue-Langevin, 71 Avenue des Martyrs, 38042 Grenoble Cedex 9 France

E-mail: vladimir.hutanu@frm2.tum.de

Pacs:

Abstract

A new polarized neutron single crystal diffractometer POLI (**Pol**arization **I**nvestigator) has been developed at the Maier-Leibnitz Zentrum (MLZ) Garching, Germany. After reviewing existing devices, Spherical Neutron Polarimetry (SNP) has been implemented on POLI as a main experimental technique using a third-generation Cryopad built in cooperation between RWTH University and Institut Laue-Langevin (ILL). In this report we describe the realization and present the performance of the new Cryopad on POLI. Some improvements in the construction as well as details regarding calibrations of Cryopad and its practical use are discussed. The reliable operation of the new Cryopad on POLI is also demonstrated.

I. INTRODUCTION

More than twenty five years after F. Tasset's development of the first Cryopad [1] and intensive works he then performed in collaboration with P. J. Brown at the Institute Laue Langevin [2], Spherical Neutron Polarimetry (SNP) is now established worldwide as an efficient method for direct characterization of complex magnetic structures that are in many cases intractable otherwise [3]. While classical polarized neutron techniques measure spin-dependent scattering cross sections (flipping ratio method, longitudinal polarization analysis and its derivatives), SNP exploits the vector properties of the neutron polarization. The changes of the polarization vector occurring upon scattering in the sample are measured. SNP

thereby allows distinguishing between polarization rotations due to the magnetic and nuclear/magnetic interactions with ordered magnetic moments and depolarization due to the presence of magnetic domains. Thus, detailed investigations of complex magnetic ground states and determinations of relative magnetic domain populations as a function of external parameters are possible using SNP.

The theoretical bases for the SNP are the general mathematical expressions of the scattering cross-sections and scattered polarization vectors derived by M. Blume [4] and S. Maleev [5] in the early sixties. About a decade later, the first experimental devices for measuring components of the neutron polarization vector were developed in Delft [6] and Gatchina [7]. They were based on resistive coils and soft magnetic shields (permalloy) and used solely for studying ferromagnetic domains by the depolarization method in the direct beam. By using a similar technical device, H. Alperin [8] performed the first experiment verifying the existence of transverse polarization components in the scattered beam and polarization rotation predicted by the Blume-Maleev equations on a magnetic Bragg reflection of the antiferromagnetic sample Cr₂O₃. He reported that it is impossible to obtain the information about antiferromagnetic domains by only measuring the scattering cross section or by analyzing the scattered polarization solely in the direction of the incident polarization. Moreover, Alperin showed that in existing devices small stray fields inside the magnetic shielding cause a significant deviation of the studied polarization from the required direction. Therefore, the sample had to be placed in a zero-field chamber to avoid unwanted precessions of the polarization and to achieve a better control of the polarization vector.

In order to improve the magnetic shielding at the sample position whilst allowing measurements at any scattering angle, F. Tasset proposed to build a polarimeter made from two concentric superconducting cylinders exploiting the Meissner effect [1]. The scattering plane is separated in three magnetically independent regions: a central part, the so called zero-field region where the sample is positioned; an annular intermediate region between the two cylinders in which two small magnetic fields created with independent superconducting coils control one spherical coordinate of the incoming and outgoing neutron polarizations; and an outside region where the remaining spherical coordinates of the incoming and outgoing polarizations are controlled with nutators. Following the development of the cryoflipper, F. Tasset adopted Nb tubes as Meissner screens because Nb is almost transparent for neutrons and does not depolarize the beam. In order to become superconducting, Nb must be cooled below 9 K, which led to the device name **Cryo**genic **Po**larization **A**nalysis **D**evice (Cryopad)

[1]. This technical development led to the elaboration of SNP as a new experimental technique that became available to ILL users [9,10].

The first mature version of Cryopad, called Cryopad-II, was then designed with a room-temperature zero-field chamber able to host a cryostat [11]. This construction decouples the cooling of the sample from that of the Meissner screens, allowing the insertion of non-magnetic sample environments into the polarimeter (cryostat, dilution refrigerator, etc.). With this setup, studies of magnetic and electric field dependence on magnetic domain populations became possible [12]. The larger diameter of the Meissner shields and the new design of the nutators permitted SNP measurements over a large scattering angle and even antiferromagnetic form factors could be measured for the first time [13].

The outstanding results in the precise characterization of complex magnetic structures like the possibility to directly distinguish between cycloidal and helicoidal magnetic orders [3,14], non-collinearity due to spin-orbit coupling and the search for "hybrid" nuclear/magnetic inelastic correlations function [15] increased significantly the popularity of SNP and the necessity to provide Cryopad devices also outside ILL. This triggered in the early 2000s the decision to build three next-generation Cryopad-III [16-20] but also other types of polarimeters. We therefore compared them with the aim to build the best possible polarized neutron diffractometer at FRM II.

II. WHICH POLARIMETER FOR POLI?

In Cryopad-II, the precessions of the incoming and outgoing polarization vectors are realized with a toroidal solenoid located between the Meissner shields and surrounded by a shorter secondary solenoid centered on the incident beam. Incoming and outgoing precession coils are coupled and the need for a precession matrix with components dependent on scattering angle limits the precision with which Larmor precessions are controlled [21]. The next generation Cryopad-III was therefore developed with the aim to decouple the precession units. After intensive calculations and the introduction of ferromagnetic yokes of high magnetic permeability at 5 K combined with Meissner screens, the design converged toward a solution consisting of a fixed and flat incoming precession unit decoupled from a partial but magnetically infinite torus outgoing coil [17]. According to the calculations the maximal deviation in the control of the polarization vector in Cryopad-III is 0.3° (curved Meissner screen) + 0.5° (precession unit) for a 25x25 mm² beam section. These performances and the

absence of interference between the coils have been demonstrated experimentally [19]. Furthermore, an outer μ -metal shielding completes the Meissner screens to further reduce the amplitude of the field in the sample space down to less than 1 mG.

Alternatively, the use of µ-metal only (no Meissner screen) to create a large zero-field chamber for hosting a sample cryostat was actively exploited in the development of Mupad (µ-metal Polarisation Analysis Device) [22,23]. The practical advantage of this SNP device is the absence of cryogenics: neither shields, nor coils are superconducting. Similarly to Cryopad, Mupad uses two independent field regions. The sample is also positioned in the center of a zero-field region, here inside the inner shield. The polarization rotations are realized in between the inner and outer magnetic shields and the coupling to the external magnetic surroundings (guide fields for the neutron polarization transport) is performed outside the outer magnetic shield. The only principal difference is that both spherical coordinates of the polarization vector are manipulated in the intermediate field region without effective magnetic shielding in between. The precession coils are decoupled by reducing their stray fields using u-metal yokes, by producing small fields inside the coils, and by ensuring a sufficiently large distance between the coils to avoid a crosstalk. Another particularity of Mupad is that µ-metal shields are ferromagnetic and may depolarize the beam passing through, in contrast to diamagnetic superconducting shields. To avoid this, relatively large openings for the incoming and outgoing beams must be provided in the magnetic shielding. As the openings should be small in order to avoid the penetration of parasitic fields inside the zero-field chamber, the complex mechanical design features many slit-segments that are opened at the desired scattering angles. In this way, the μ-metal shield becomes an active mechanical component that is moved and supports stress and friction due to the tight mechanical contact necessary for efficient magnetic shielding. Because magnetic properties of u-metal strongly depend on the mechanical stress collected during the assembly and the exploitation, it becomes difficult to guarantee a perfect reproducibility and precise polarization manipulations at all scattering angles. To avoid high currents in the resistive coils, Mupad is also better suitable for usage with cold neutrons [24] and it has been successfully implemented on the cold triple axis spectrometer TASP@PSI and the very cold instrument MIRA@MLZ [23]. After testing Mupad with 1.165 Å neutrons on the hot source of the FRM II [24] the decision was taken to build a Cryopad-III for the new polarized diffractometer POLI [25,26]. This decision was motivated by the compact design (important limitation at MLZ), the midterm support offered by ILL for constructing the device and exploiting the SNP technique, the economical aspect (both devices have comparable

acquisition costs) and the higher technical performances. Indeed, the absence of moving μ-metal shields ensures better field screening, the coupling coils of Mupad had to be upgraded to address the short wavelengths used on POLI, and there is no phase shift due to parasitic fields inside the coil area of Cryopad [24]. The new Cryopad installed on POLI@MLZ is very similar to the Cryopad-III used on D3 and newly also on ThALES at ILL. However some improvements were introduced which are discussed in the next section. It has been successfully realized in cooperation between RWTH Aachen University and ILL and commissioned in 2010-2011 [27]. First scientific results were recently published [28-31] and others are in preparation.

In parallel, the number of experiments and high-ranking publications using SNP techniques has increased continuously. The technique became of general interest at several neutron scattering facilities both in Europe and oversees [32-35]. This also led to new technical developments in the field. Most of them concentrated on the development of smaller and cheaper devices that would not require cryogenic liquids but use "dry" cryostats. For example at University of Indiana (USA), a project for developing a cryogenic SNP device for time-of-flight instrument based on the Cryopad concept and high-T_c superconducting YBCO Meissner shields cooled down with a closed-cycle refrigerator started [36]. The first prototype called CryoCUP has demonstrated the feasibility of using YBCO foils as Meissner shields in neutron beams and provided rather good control of the polarization vector, especially for neutrons with 2-8 Å (dephasing factor less than 2%). However this compact device is presently limited in its scattering angle range to direct transmission and SANS measurements. Moreover, similar to the first Cryopad, the same cryostat controls the temperature of both the sample and Meissner shields, limiting the sample temperature range to 20-80 K [37].

Another newly reported miniaturized SNP device, called miniMupad [38,39], in some extend also goes back to the Cryopad-I design where small precession coils are positioned close to the sample inside the cryostat. Here, similarly to the large Mupad, the static coils are shielded with μ -metal yokes and decoupled by an appropriate distance between them. This device was built for SNP in SANS mode, therefore accepting a maximum scattering angle of 15°. The reported accuracy of the polarization control is about 3° for the direct beam and cold neutrons [38]. One of the targeting benefits of such devices in comparison to the "classical" Cryopad using Nb is the absence of liquid cryogens refills. However, the consumption of cryogens and related work during experiments with the present Cryopad are rather moderate as shown below.

In spite of these recent and interesting developments in the field of SNP instrumentation, we consider that Cryopad-III remains until today the most precise, robust, reliable and mostly used device for SNP. In the next sections we explain the reasons for this. Being regularly asked by the polarized neutron community, especially about the details of its routine operation e.g. [32-35], we present a detailed report about the development and operation of the most recently built Cryopad used on the single crystal diffractometer POLI at MLZ. We focus on the practical aspects of the daily operation and details that are either not described or solved differently for this version in comparison with other Cryopad-III devices built earlier [19,20]. We hope this report will be useful to both users and developers of future SNP devices.

III. IMPROVED IMPLEMENTATION ON POLI



FIG. 1. Main components of the new Cryopad produced by different companies; a) cryostat made by AS Scientific, Oxfordshire, UK, b) precession coils frame made at IFF workshop FZ Jülich, Germany c) μ -metal shields made by Magnetic Shields Ltd, Kent, UK, d) Nb Meissner screens produced by SDMS, Saint-Romans, France, e) outgoing superconducting precession coil wound at ILL, France.

RWTH Aachen University acquired from ILL a license for reproducing a copy of Cryopad-III for the new diffractometer POLI at MLZ (FRM II). Additionally a scientific collaboration agreement between ILL and RWTH for the realization of this polarimeter and its implementation on the new instrument in Garching was signed. In order to reduce the costs, the manufacturing of the main components was subcontracted following a tendering procedure managed by RWTH using ILL original drawings. The final assembly and tests of

the new Cryopad were then performed at ILL. The implementation of the whole SNP setup including Cryopad, nutators, controlling electronics, and auxiliary devices on the POLI diffractometer as well as the training of the RWTH personal in using Cryopad were performed at MLZ in Garching with participation of ILL co-authors.

The detailed view of the Cryopad-III design has already been published elsewhere [17]. The main components are: a cryostat with its liquid He and N_2 reservoirs, two superconducting shields made from Nb with residual resistance ratio of at least 40, two superconducting Larmor precession coils mounted between the Nb shields, external μ -metal shields for operation, cooling and storage, incoming and outgoing nutators and afferent electronics for powering the coils, monitoring the cryogens levels and the Nb temperature, etc. The main subcontracted components are shown in Figure 1.

As explained above, the incident and outgoing Larmor precession coils are fully decoupled in Cryopad-III. However, because of the unavoidable presence of gaps between Nb shields and stray fields produced by soft-magnetic yokes, the field produced by the outgoing precession coil slightly leaks into the zero-field region to a level of 0.13 mG/A i.e. 0.02° unwanted Larmor precession at 1 Å. We therefore added Nb caps on top and bottom of the superconducting Nb shields (Fig. 1d) to fully close the volume. Measurements performed with our fluxgate magnetometer demonstrate that the magnetic leakage was cancelled (< 0.01 mG/A).



FIG. 2. SNP setup using Cryopad on POLI: (1)- polarizer with 3 He cell, (2)- incoming nutator, (3)- Cryopad in μ -metal shield, (4)- fixing ring, (5)- outgoing nutator, (6)- Decpol analyzer with 3 He cell and detector, positioned on the rotating detector arm (7).

In Figure 2, we present the Cryopad fixed above the rotating sample table of the POLI diffractrometer. The non-polarized monochromatic beam coming from the right is polarized along the neutron propagation direction by the ³He spin filter inside the polarizer cavity (1). This polarization is turned adiabatically into the plane normal to the neutron beam direction by the incoming nutator attached to the polarizer (2). If necessary, this polarizer can be moved along the beam axis. The Cryopad (3) is centered on the sample axis and fixed on a dedicated ring (4) aligned with a level. On the detector arm (7) the ³He polarization analyzer Decpol (6) [17,26] and its outgoing nutator (5) receive the beam scattered by the sample. Decpol also features a linear translation stage parallel to the beam to adjust its position as close to Cryopad as feasible to ensure adiabatic transport of the polarization and minimize aberrations revealed by simulations. The detector arm (7) with Decpol (6) rotates around the sample position. The accessible scattering angle 2θ ranges from -10° to +120°.

The second improvement is related to the manipulation of the nutators. We kept their original magnetic design that is linked to the design of the Meissner screens [17], but changed their mechanical drive. New backlash-free geared belt drives were designed and implemented for both the incoming and outgoing nutators (Fig. 3). These new rotating plates provide higher velocities compared to the original systems used at ILL. The speed reaches about 45°/s whilst ensuring an angular position of the nutator with a precision better than 0.1° and repeatability of better than 0.05°. These higher speed mechanics reduce dead times during experiments by a factor of 5 on a diffractometer where polarization directions are often changed.



FIG. 3. Incident nutator fixed at the exit of the polarizer. A backlash-free geared belt (1) with transmission driven by a stepper motor (2) rotates the nutator (3) around the beam axis. On the same belt-loop a high resolution optoelectronic encoder (4) controls the angular positioning. Angular precision of better than 0.1° is achieved with a gear ratio of five.

To reduce the penetration of the earth's magnetic field and stray fields from magnetized components like sample table, mechanics, motors, etc. situated below the Cryopad, a series of μ-metal shields are employed as shown on Figure 4. Above and below the scattering plane, μmetal shields surround the Cryopad. These shields (1) and (5) are linked magnetically using an overlap (9) to facilitate the environmental magnetic field circulation (magnetic shortcut). A μ-metal pot (7) closes magnetically the zero-field chamber (sample space) of Cryopad at the bottom. The sample cryostat (3) is inserted inside the Cryopad and attached to the rotating goniometer through this µ-metal pot (7). On POLI, just as on D3 at ILL, this is realized by evacuating a volume on the surface that is large enough to produce the force necessary to hold the cryostat (perfect magnetic screening with no hole in the µ-metal). The gap between the fixed lower shield (5) and the movable μ -metal pot (7) is chosen in order to assure a magnetic connection and allow the tilting of the cryostat inside the Cryopad by up to $\pm 4^{\circ}$. That way, some flexibility is provided for a precise sample alignment with the scattering plane. This option has proven to be very useful, significantly reducing beam-time losses during SNP experiments. The need for sample reorientation capabilities inside Cryopad was recognized long ago because the determination of complex magnetic configurations requires access to Bragg peaks not belonging to the same scattering plane. A miniaturized Eulerian cradle mounted inside a cryostat was proposed [17] and recently realized at ILL [40]. Alternatively, we successfully demonstrated on POLI [41] that non-magnetic miniaturized piezo-motors extend the tilting angle and provide precise alignment of the sample in the "dry" cryostat installed inside the Cryopad.

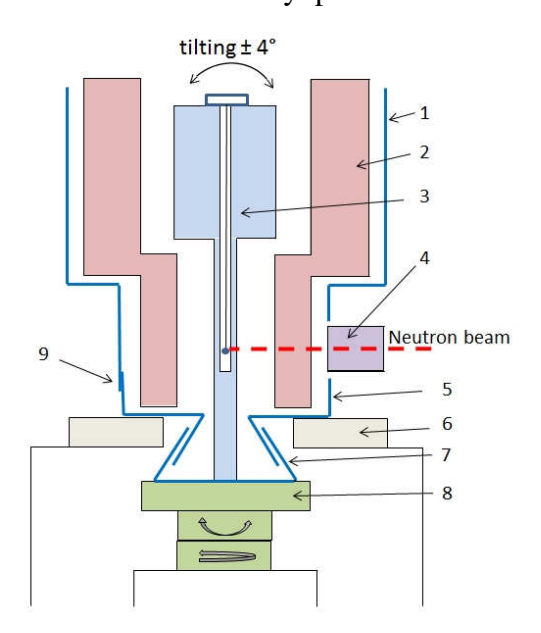


FIG. 4. Sketch showing additional μ -metal shields around the Cryopad on POLI: 1- upper μ -metal shield, 2- Cryopad, 3- sample cryostat, 4- nutator, 5- lower μ -metal shield, 6- fixing ring, 7- movable μ -metal pot, 8- sample table POLI, 9- overlapping μ -metal shields (see text).

The intense direct beam hits the Cryopad screens twice (entrance and exit) and cross a nonnegligible amount of different materials: 4 mm of pure Nb, 10 mm of Al, and 0.4 mm of NbTi superconducting wires. In order to evaluate the amount of background created by the Cryopad, a 20 scan of the detector around Cryopad without sample was performed. The results in Figure 5 show a significant increase of the background at small angles around the direct beam. In order to improve the situation, an absorber made of boron-doped rubber was placed inside the zero-field chamber in front of the direct beam but of course behind the sample. The comparison of scans measured with and without beam-stop demonstrates its high usefulness. The background is reduced at all measured 20, and more pronouncedly at lower angles where the gain factor reaches 15 (inset of Figure 5). The residual peak around $2\theta=23^{\circ}$ is due to 0.9 Å neutrons scattered by the incident aluminum screens and cannot be suppressed. The significant reduction of the background in the lower 20 region is very beneficial for the measurements on weak incommensurate magnetic peaks. The usage of the beam-stop inside Cryopad has become standard on POLI and is strongly recommended to users of other Cryopad and Mupad devices. Of course, as boron-doped rubber is not very efficient at the very short wavelengths, a ceramic B₄C plate is preferable below 0.7 Å.

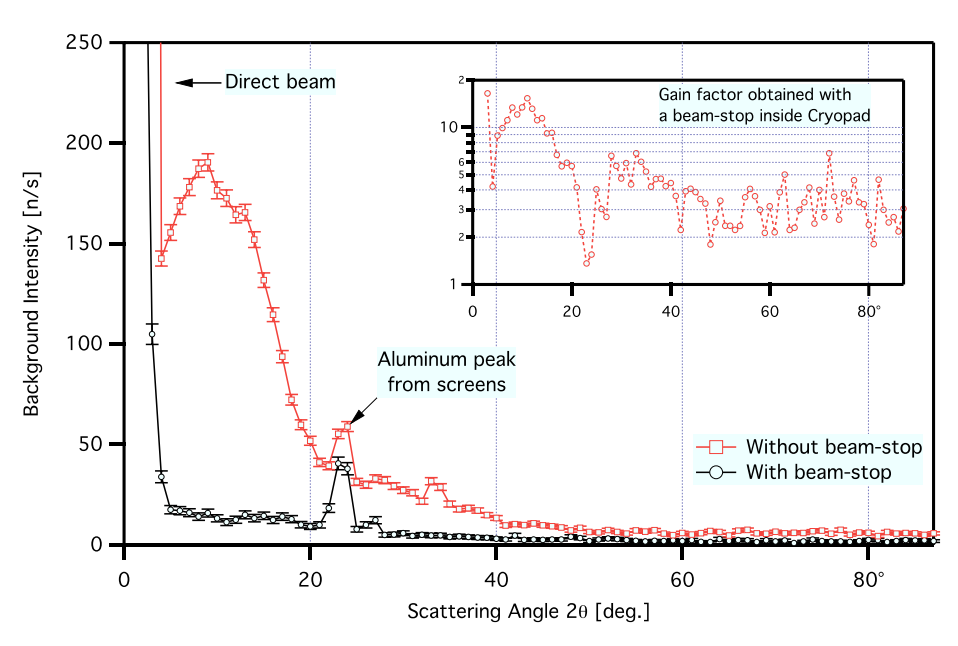


FIG. 5. 2θ scans with and without beam-stop inside the Cryopad performed at 0.9 Å. The peak at $\approx 23^{\circ}$ corresponds to neutrons scattered by aluminum screens and cannot be suppressed. The gain factor shown in the inset exceeds 10 at low scattering angles and averages to about 3 above 40° .

IV. CALIBRATION OF THE NEW CRYOPAD

A standard calibration procedure of Cryopad-III e.g. on D3 at ILL is described elsewhere [20]. A four-step process using software macros is proposed: 1) alignment of the nutators relative to each other, 2) calibration of the incoming and 3) outgoing Larmor precession coils, and 4) alignment of the nutators with the precession fields. Either the direct beam (no sample used) or the diffracted beam (from a nuclear Bragg peak on sample) can be used. Our experience shows that a diffracted beam offers a slightly higher precision because of the better monochromatization of the scattered beam. Despite the use of a harmonic filter, the incident beam of POLI is partially contaminated (about 2.5%) with epithermal neutrons from the hot source. The usage of a ³He spin filter as polarizer leads to different polarizations for the desired monochromatic and the spurious higher energy neutrons. Using a nuclear Bragg reflection of a sample, only the monochromatic part satisfying the Bragg relation is selected and the scattered polarization is better defined. The intensity from the direct beam is higher than that of the diffracted one and could provide better statistics in shorter time but it saturates the detector and makes the use of an attenuator mandatory. Thus, using a strong nuclear Bragg reflection from a well-known sample, the calibration procedure is almost as quick as in the direct beam, and provides the same results with better precision. One may note that as the first three calibration steps are independent, they can be performed in arbitrary order.

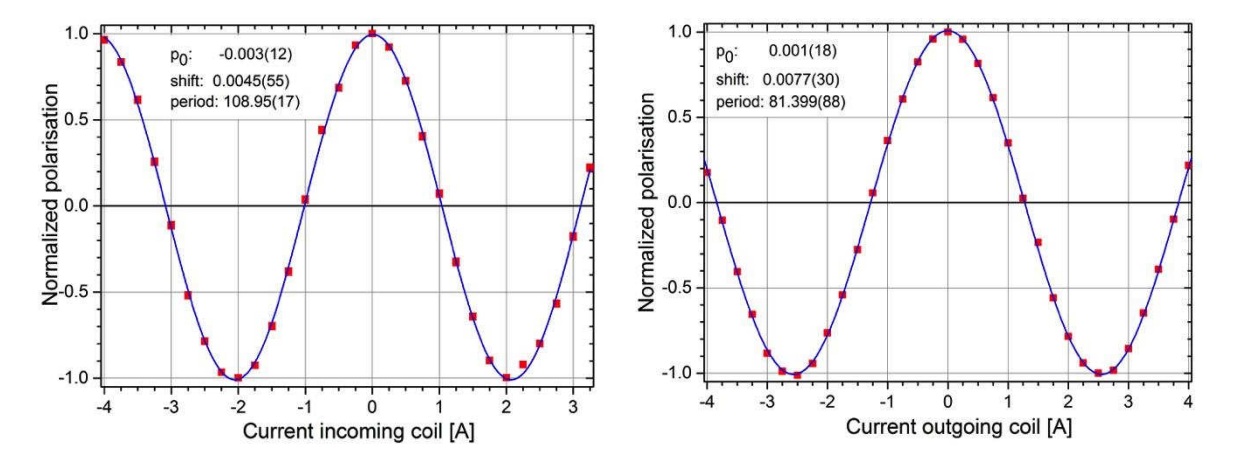


FIG. 6. Typical calibration curves for the incoming (left) and outgoing (right) precession coils, measured at a wavelength of 0.794 Å. Red points are experimental data (error bars smaller than symbols) and blue lines are cosine fits determining offsets and precession amplitudes in [°/A Å].

On POLI, we generally start with the calibrations of the precession coils. The current is injected in the incident coil with a bipolar power supply from minimal to maximal value in discrete steps (with the other coil current set to zero), and the polarization of the direct beam

is recorded as a function of current. The result is fitted with a cosine function and the amplitude of the Larmor precession determined in degrees per Ampere and Å. The procedure is then repeated with the outgoing coil. Of course, this calibration assumes that the wavelength of the beam is well known and the maximum amplitude of the measured polarization depends on the polarization efficiencies of the spin polarizer and analyzer. Figure 6 shows the results of the precession coil calibrations of the new Cryopad on POLI. From the two pictures, it is easy to observe that a 1 A current injected in the incident coil rotates the polarization stronger than the same current in the outgoing coil. This is related to the coil geometries: same neutron path but different heights and number of loops. The absolute values of the precession amplitude for the incoming and outgoing coils of the new Cryopad in comparison to the earlier versions of the Cryopad-II and Cryopad-III are presented in Table 1. In the older Cryopad-II, precession fields being superposed, the incident and outgoing precessions angles were calculated from a non-diagonal precession matrix with a coefficient varying with the detector position [21]. In Cryopad-III devices, the precession coils are magnetically decoupled and the canceling of the non-diagonal terms a_{12} and a_{21} was confirmed by calibrations performed on different Bragg reflections and wavelengths. The calibration of the coils is easier (no need to rotate Cryopad) and the precessions are controlled with better accuracy. The new Cryopad on POLI, having the same dimensions as ones used on D3, exhibits also similar precession amplitudes. The two more compact polarimeters built for inelastic scattering present smaller precession amplitudes because they were designed for thermal neutron beams.

Cryopad/Instrument@Facility	a ₁₁	a ₁₂	a ₂₁	a ₂₂
	°/(A.Å)	°/(A.Å)	°/(A.Å)	°/(A.Å)
Cryopad-II - IN20@ILL	-93.997	-40.97	a ₂₁ (γ) *	40.97
Cryopad-III - IN22@CEA	84.93	0	0	30.48
Cryopad-III - TAS-1@JEARI	92.17	0	0	30.11
Cryopad-III - D3@ILL	123.65	0	0	76.50
Cryopad-III - POLI@MLZ	109.89	0	0	81.55

Table 1. Coefficients a_{ij} of the precession matrices determined from calibrations of existing Cryopad. This 2x2 matrix is used to calculate the incident and outgoing precession angles as a function of currents injected in the coils. Only Cryopad-II presents the non-diagonal terms a_{12} and a_{21} as its precession coils are superposed. Here $a_{21}(\gamma)$ =4.1386 - 0.1222 γ^2 + 0.7406 γ^4 , where γ is the angular detector position in radians [21].

The values shown in Table 1 for the third-generation Cryopad only depend on the coil construction and they are independent of wavelength, scattering angle and stray field. We performed independent calibrations of the precession coils using different wavelengths and

experimental setups at different times on POLI. Figure 7 presents the results of these calibrations. They demonstrate the wavelength independence and reliability of the precession coils.

Cryopad is a very robust and reproducible device. Once calibrated, there is no need to repeat the procedure, as long as no significant changes are performed inside the device. Even after repeated warming up and re-cooling of the Cryopad, crane transportations, multiple installations and dismounting of the Cryopad on the instrument over the years, the calibrated values of the coils have not changed. There is no visible aging effect. Applying known precession amplitudes (Table 1) for the fit in the Figure 6, Cryopad can even be used to calibrate quickly the incident wavelength of the diffractometer POLI in the direct beam.

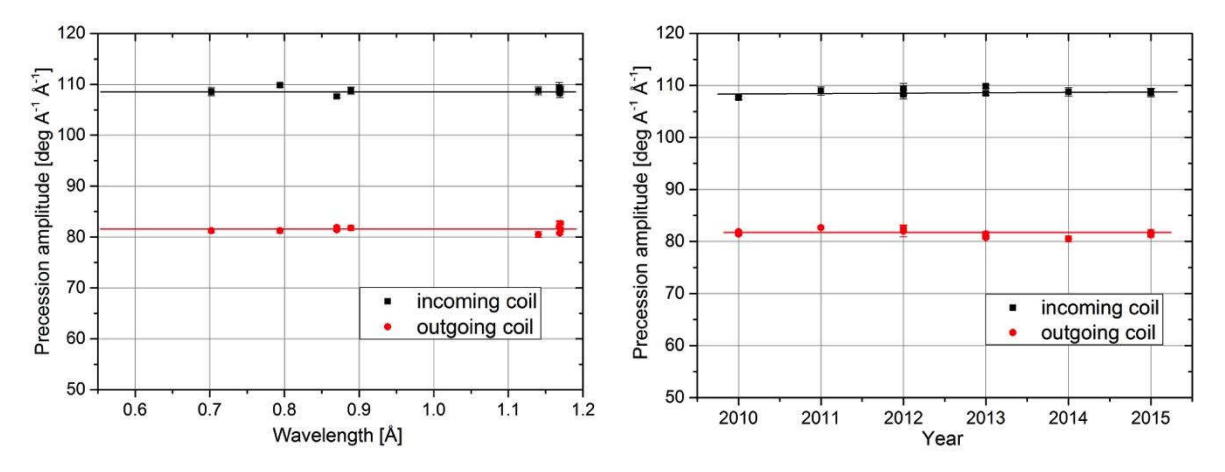


FIG. 7. Larmor precession amplitudes measured in the incoming and outgoing coils of the new Cryopad on POLI vs. wavelength (left) and over the time after repeated installations and dismounting (right). Solid points are experimental results obtained from fits like those shown in Figure 6. The continuous lines are linear fits to the experimental data showing no wavelength dependence and no time dependence or aging effects.

After the calibration (or just verification) of the precession coils, the alignment of the guide fields of the nutators relative to each other, called also the "perpendicularity of the nutators" in Ref. [20], is performed. Basically, this calibration ensures that both the incoming and outgoing guide fields are perfectly parallel when tuned toward the same axis (e.g. the axis Oz perpendicular to the scattering plane of the instrument). In Figure 8a, precession currents are set to zero, the outgoing nutator is tuned toward Oz, and the incident nutator is rotated. The polarization is measured as a function of its angular position. One obtains a perfect cosine curve with a periodicity of 360°. The shift of the maxima near zero degree position, or the more easily observable shift of the intercept point between the fit curve and zero polarization near the 90° position, gives the angular offset between the fields produced by the nutators. This offset is of purely mechanical origin and is corrected by simply readjusting the offset

value of one of the nutator encoders. A precision in the alignment of the nutators of 0.1- 0.2° is easily reached on POLI. A quicker calibration consists in measuring a small part of the total 360° cosine curve centered on the 90° position, e.g. $90^{\circ} \pm 15^{\circ}$.

While in the first three steps of the calibration of Cryopad, the precession coils and nutators are calibrated independently; the last step determines the alignment of the fields produced by the nutators relative to the fields produced inside the precession coils. Because nutators were aligned with respect to each other, it suffices to align the incoming nutator with the incoming precession coil. To maximize the sensitivity with which this calibration is performed, we rotate the incoming polarization vector by 180° with the precession coil and measure the transverse component of the rotated polarization. Note that the precise corresponding current value is known from the first calibration (Table 1). The nutators are then oriented perpendicular to each other and rotated synchronously around the 90° position of the incoming nutator. If the system is perfectly calibrated, the outgoing polarization is zero at the 90° position (Figure 8b). The measured offset is corrected by applying the same angular offset to both nutators. On POLI an offset lower than 0.1° is reached.

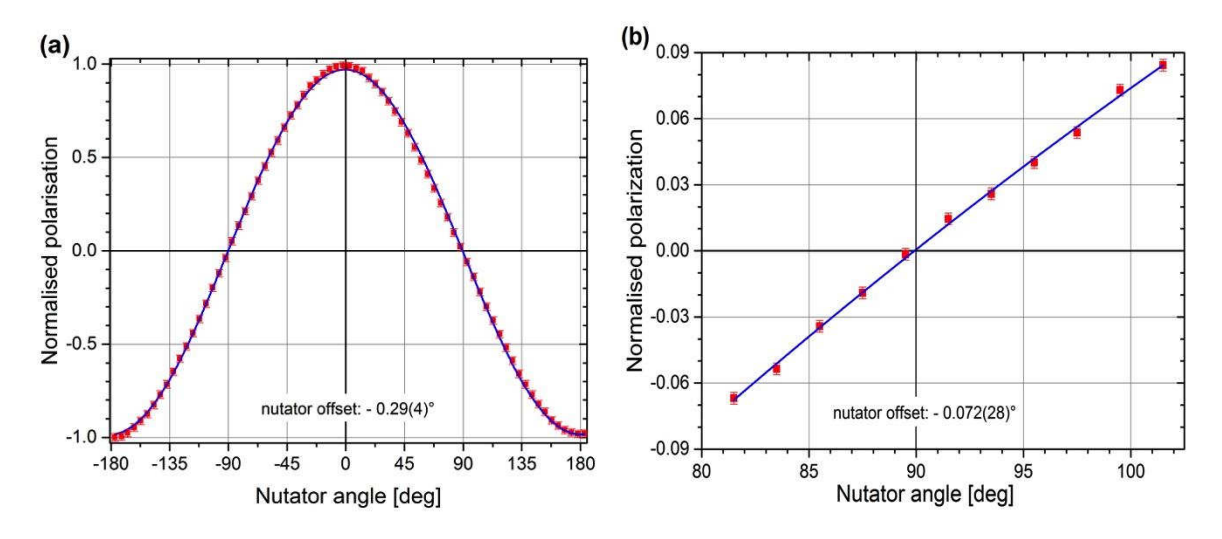


FIG. 8. (a) Calibration of the alignment of the guiding fields of the nutators relative to each other. The outgoing polarization is measured as a function of the angular position of one nutator, while the other one is oriented along Oz. As an example, results for a slight misalignment of about 0.3° are shown. (b) Quick calibration of the alignment of the field produced by nutators with the one produced by the incoming precession coil. A perfect alignment is obtained if the polarization is null at 90°. Red points are experimental data. The blue curve is a cosine fit to the data determining the misalignment.

Performing a similar procedure for the outgoing nutator and precession coil will not improve further the alignment. However, it is used once to cross check the parallelism of the fields produced by the incoming and outgoing precession coils. If the co-planarity of the precession fields is not satisfactory, the Cryopad may be opened and the incident precession coil is tilted

mechanically to correct the misalignment. Our measurements show that this misalignment is of about 0.3° in Cryopad-III device on POLI. When the instrument features a position sensitive detector, it is also possible to check the co-planarity of the precession fields with the scattering plane. This is performed once and mechanically fixed by modifying the support of the Cryopad.

From the results of these calibrations, we can estimate a maximum deviation in the absolute control of the polarization vector using Cryopad on POLI. Combining the measured precision in the positioning of both nutators and the maximal possible offset between them, one ends up with a maximal total uncertainty of 0.4°. This is comparable to the absolute offset of 0.3° determined for the misalignment of the precession coils inside the Cryopad. The precision with which the Larmor precessions are controlled inside the precession coils is limited by the performances of the bipolar power supplies. Properly calibrated Kepco BOP analog amplifiers provide a precision and reproducibility of the current control that is better than 0.5 mA for currents below 1.5 A. From the calibrations of the coils, we deduce that 1 mA deviation corresponds to about 0.1° Larmor precession. Combining all these errors and taking into account a measured magnetic field in the zero-field chamber of less than 2 mG one finds out that the control of the polarization vector on POLI using the new Cryopad is performed within accuracy of better than 1°. Taking into account large scattering angle up to 120° and short wavelength used on POLI (below 1 Å) this performance is yet unreachable by any other SNP device type.

V. CRYOPAD IN PRACTICE

Figure 9 shows the Cryopad in the "parking" position between experiments. The electronics cabinet (1) is shown on the left. It includes all power supplies, not only for the Cryopad and the nutators, but also for the 3 He polarizer and analyzer as well as the temperature and cryogen level monitors and a computer with hardware-control drivers for conducting SNP experiments. On the right, the Cryopad (2) is shown inside the μ -metal box (3) for cooling but also used for storage and transportation.

To avoid trapping magnetic field inside the zero-field region upon cooling below the superconducting transition in the Nb Meissner screens, it is necessary to put the Cryopad into a μ -metal box that shields environmental fields. A fluxgate magnetometer is positioned inside the Cryopad approximately at the sample height to monitor the fields during the cooling. To achieve the needed near-to-zero-field, Cryopad is moved with the trolley box toward a

position in the experimental hall with the smallest available stray field, and cooled down with liquid He at that position. Values of 1-2 mG are typically reached, two orders of magnitude lower than the geomagnetic field of about 350 mG. The μ -metal box is closed at the bottom and high enough to minimize field penetration down to the sample position. After cooling below the superconducting transition, the Meissner effect freezes the integrated flux of magnetic field penetrating the cylinder. Afterwards, the Cryopad can be moved away and taken out of the μ -metal box without risk as long it remains cold. The field measured inside Cryopad after installation on POLI is of the same amplitude as in the cooling box.

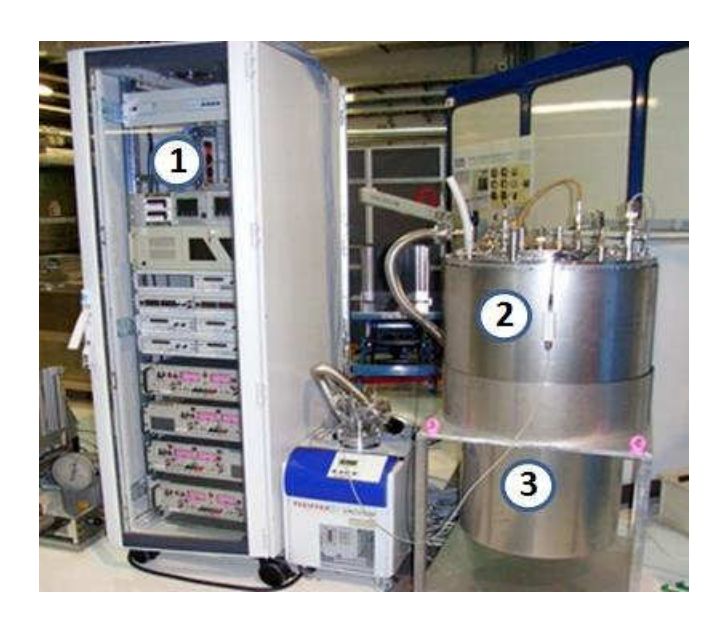


FIG. 9. Cryopad in its μ -metal cooling box. (1) Electronics cabinet for housing all power and control devices, (2) Cryopad situated inside the μ -metal "barrel" (3) on trolley.

The Cryopad is cooled down in two steps, similar to any cryostat. First, in order to save liquid He (LHe), liquid nitrogen (LN₂) is injected overnight into the LHe reservoir until the system reaches about 80 K. Then, after a careful flush with He gas, the liquid helium bath is cooled down and then filled to reach the base temperature (4.2 K). The volume of LHe necessary to cool the Cyopad down depends on the speed of the cooling process. On POLI, during a typical cool-down time of about 3 hours, about 70 liters of LHe are used. Afterwards, the boil-off ratio is of about 9% per day. Figure 10 shows measured LHe and LN₂ consumption curves under standard conditions. The LHe autonomy of our Cryopad is slightly higher (10-11 days) compared to the specified value of 7-8 days based on the experience with previous Cryopad-III devices e.g. in Ref. [19]. As a typical experiment duration using Cryopad on POLI being of 5-8 days, the refill is scheduled between two experiments. The LN₂ bath is refilled automatically about every 19 hours as shown in Figure 11a, using a level-meter relay and an

electromagnetic valve on the top of the LN₂ tank situated outside the experimental area so that it can be refilled without pausing the experiment. The consumption per refill is about 25 l both for LN₂ and LHe. As shown in Figure 11b, when the LN₂ supply fails, the consumption of LHe increases but the system still remains cold and operates normally for many hours. Thanks to this, there is always enough time to fix potential errors and refill the LN₂ bath without disturbing the experiment. That would not be the case with a closed-cycle refrigerator. Moreover, because of the low LHe consumption, it would take about 10 years of permanent use to cover the acquisition cost of a closed cycle refrigerator assuming 200 days of operation per year and without considering additional running costs.

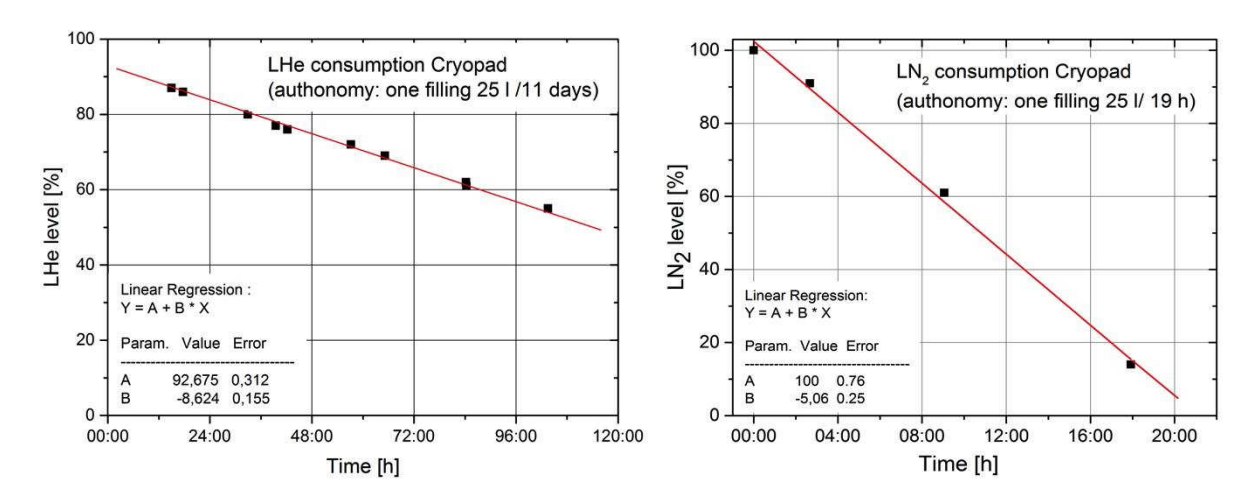


FIG. 10. Consumption curves of LHe (left) and LN_2 (right) in Cryopad on POLI. Black points are measured data, the red line is a linear fit. The results from the fitted boil-off rates are less than 9 % /day for LHe and about 5 % /h for LN_2 .

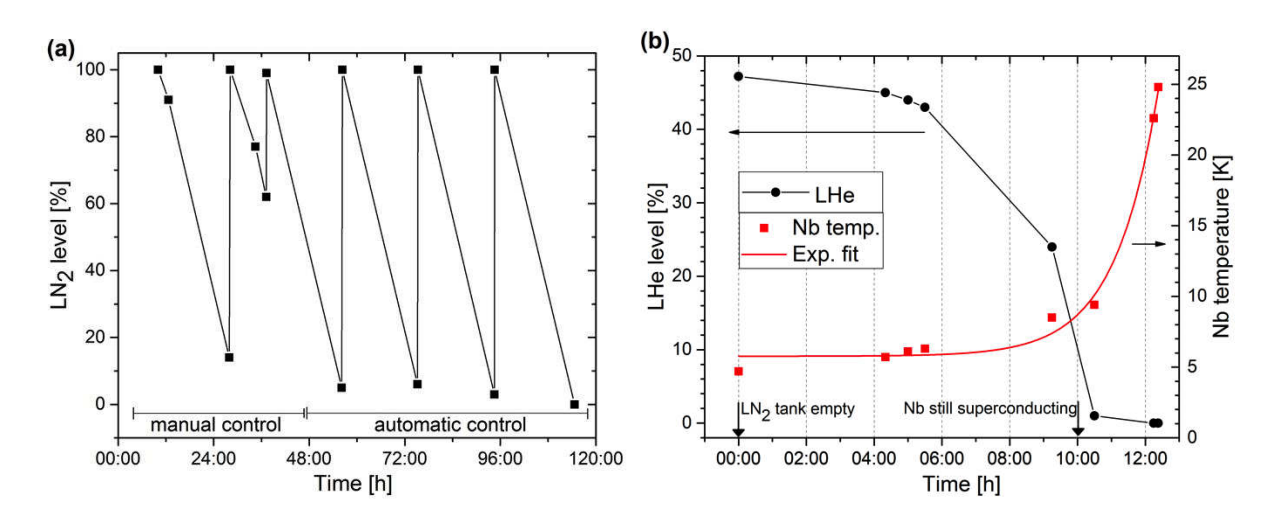


FIG. 11. (a) Automatic refilling of LN₂ in Cryopad on POLI. Manual control is also possible. (b) Warming up of the Cryopad without LN₂. Solid points are measured values, the red curve is an exponential fit to the temperature data, horizontal arrows indicate corresponding scales and vertical arrows denote times between which the Cryopad remains operational without

LN₂. In the shown example starting from 48 % LHe, normal operation over 10 h was reached. In both (a) and (b) black lines are just guides to the eyes.

On its way through the Cryopad, we have seen that the incident neutron beam crosses a non-negligible amount of different materials. Those materials are transparent to the polarization and low absorbers. The intensity of the same Bragg reflection from the same sample was measured with and without Cryopad at 0.79 Å and 1.17 Å wavelengths to determine its transmission. Figure 12 shows the results of this comparison at one of the tested wavelengths. As expected, a reduction of the peak intensity is observed. The total transmission calculated as the ratio of integral intensities collected with and without Cryopad amounts to 76% for 1.17 Å neutrons. A similar but slightly better transmission is measured for the shorter wavelength. This is comparable to the transmission of e.g. a low-field cryomagnet.

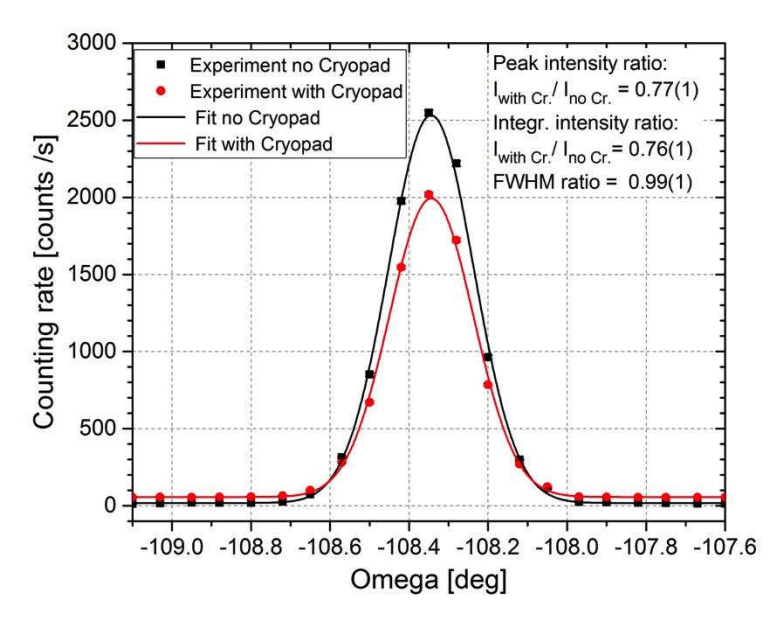


FIG. 12. Rocking curves of the Si (202) Bragg reflection with and without Cryopad on POLI. Solid points are measured intensities (error bars are smaller than symbols) and curves are Gaussian fits. A transmission of 76% is determined at 1.17 Å.

VI. CONCLUSION

SNP is a very powerful technique being adopted at several neutron facilities. Despite significant technical developments performed in recent years in this field, Cryopad remains the most precise and robust polarimeter. A fourth copy of the third generation Cryopad has been realized in cooperation between ILL and RWTH Aachen University and successfully implemented on the new hot-beam polarized-neutron diffractometer POLI at MLZ in

Germany [42]. Several technical improvements were performed to increase further the reliability, performance and facilitate it standard use: fully closed Meissner cavity, faster nutator drives, µ-metal shielding allowing sample movements inside Cryopad and internal beam-stop reducing the background. The performance of the new Cryopad on POLI has been evaluated and the absolute precision with which the polarization vector is controlled is routinely better than 1° after quick straight calibrations. It was experimentally proven from a number of experiments [28-31] using different wavelengths, experimental conditions and setups that the new Cryopad is very robust and reliable, requires low maintenance and features moderate running costs. It is provided with dedicated control software allowing the remote control of all required parameters. User-friendly SNP experiments are now accessible on the diffractometer POLI to the broad user community [43].

ACKNOWLEDGEMENTS

We are grateful to J. Krüger for support in setting up the control software for the new Cryopad. The work has been supported by German Ministry for Education and Research BMBF through the projects 03HE6AA3, 03HE7AAC, 05KN7PAA and 05K10PA2.

References

¹F. Tasset, Physica B: Condens. Matter **156**, 627 (1989).

²P.J. Brown, T. Chatterji, *Neutron Scattering from Magnetic Materials* (Elsevier Science, Amsterdam, 2006) p. 215–244.

³P.J. Brown, Physica B Condens. Matter **297**, 198 (2001).

⁴M. Blume, Phys. Rev. **130**, 1670 (1963).

⁵R.A. Suris, S.V. Maleyev, V.G. Bar'yakhtar. Sov. Phys. -Solid State 4, 2533 (1963).

⁶M. Th. Rekveldt. J. Phys. Paris **32**, C579 (1971).

⁷V.I. Volkov, A.G. Gukasov, A.I. Okorokov, V.V. Runov, Journal of Experimental and Theoretical Physics **42**, 590 (1975).

⁸H. Alperin, in *Proceedings of ICM-73*, Moscow, Soviet Union, volume III, (1973) p. 128.

⁹V. Nunez, P.J. Brown, J.B. Forsyth, and F. Tasset, Physica B: Condens. Matter **174**, 60 (1991).

¹⁰P. J. Brown, J. B. Forsyth, and F. Tasset. P. Roy. Soc. Lond. A Mat., 442147, 160 (1993).

¹¹F. Tasset, P.J. Brown, E. Lelièvre-Berna, T. Roberts, S. Pujol, J. Allibon, and E. Bourgeat-Lami. Physica B: Condens. Matter **267-268**, 69, (1999).

¹²P.J. Brown, J. B. Forsyth and F Tasset J. Phys.: Condens. Matter **10**,663 (1998).

¹³P.J. Brown, J.B. Forsyth, and F. Tasset, Physica B: Condens. Matter **267**, 215 (1999).

¹⁴P J Brown, J B Forsyth, E Lelièvre-Berna, and F Tasset, J. Phys.: Condens. Matter **14**, 1957 (2002).

¹⁵L.P. Regnault, H.M. Ronnow, J.E. Lorenzo, R. Bellissent, and F. Tasset, Physica B: Condensed Matter **335**, 19 (2003).

- ¹⁶E. Lelièvre-Berna and F. Tasset, Physica B: Condens. Matter **267**, 21 (1999).
- ¹⁷Eddy Lelièvre-Berna, in *Proc. SPIE 4785: Advances in Neutron Scattering Instrumentation*, Seattle, US, 2002, edited by Ian S. Anderson and Bruno Guérard (2002) pp. 112–125.
- ¹⁸L.P. Regnault, B. Geffray, P. Fouilloux, B. Longuet, F. Mantegezza, F. Tasset, E. Lelièvre-Berna, E. Bourgeat-Lami, M. Thomas, Y. Gibert, Physica B: Condensed Matter **335**, 255 (2003).
- ¹⁹M. Takeda, M. Nakamura, K. Kakurai, E. Lelièvre-Berna, F. Tasset, and L.-P. Regnault, Physica B: Condens. Matter **356**,136 (2005).
- ²⁰E. Lelièvre-Berna, E. Bourgeat-Lami, P. Fouilloux, B. Geffray, Y. Gibert, K. Kakurai, N. Kernavanois, B. Longuet, F. Mantegezza, M. Nakamura, S. Pujol, L.-P. Regnault, F. Tasset, M. Takeda, M. Thomas, and X. Tonon, Physica B: Condens. Matter **356**,131 (2005).
- ²¹F. Tasset, E. Lelièvre-Berna, T.W. Roberts, E. Bourgeat-Lami, S. Pujol, and M. Thomas, Physica B: Condens. Matter **241**, 177 (1997).
- ²²M. Janoschek, Diploma thesis, Technische Universität München, Munich (2004).
- ²³M. Janoschek, S. Klimko, R. Gaehler, B. Roessli, and P. Boeni, Physica B: Condens. Matter **397**, 125 (2007).
- ²⁴V. Hutanu, M. Janoschek, M. Meven, P. Boeni, and G. Heger, Nucl. Instrum. Meth. A **612**, 155 (2009).
- ²⁵V. Hutanu, M. Meven, and G. Heger, Physica B: Condens. Matter **397**, 135 (2007).
- ²⁶V. Hutanu, M. Meven, E. Lelièvre-Berna and G. Heger, Physica B **404**, 2633 (2009).
- ²⁷V. Hutanu, M. Meven, S. Masalovich, G. Heger, and G. Roth, J. Phys.: Conf. Ser. **294**, 012012 (2011).
- ²⁸V. Hutanu, A. P. Sazonov, M. Meven, G. Roth, A. Gukasov, H. Murakawa, Y. Tokura, D. Szaller, S. Bordacs, I. Kezsmarki, V. K. Guduru, L. C. J. M. Peters, U. Zeitler, J. Romhanyi, and B. Nafradi, Phys. Rev. B **89**, 064403 (2014).
- ²⁹J Stein, M Baum, S Holbein, T Cronert, V Hutanu, A C Komarek, and M Braden, J. Phys.: Condens. Matter **27**, 446001 (2015).
- ³⁰M. Baum, PhD thesis, University Köln, Cologne, Germany (2013).
- ³¹P. Schmakat, PhD thesis, Technische Universität München, Munich, Germany (2015).
- ³²K. Siemensmayer (private communication, 2012).
- ³³M. Braden, A. Grünwald, J. Stein (private communication 2012, 2014).
- ³⁴R. Pynn (private communication 2010).
- ³⁵P. Cheng (private communication 2014, 2016).
- ³⁶T Wang, F Li, S R Parnell, W A Hamilton, H Kaiser, A L Washington, D V Baxter, and R Pynn, J. Phys.: Conf. Ser. **528**, 012024 (2014).
- ³⁷T. Wang, S. R. Parnell, W. A. Hamilton, F. Li, A. L. Washington, D. V. Baxter, and R. Pynn, Rev. Sci. Inst. **87**, 033901 (2016).
- ³⁸Jonas Kindervater, Diploma thesis, Technische Universität München, Munich (2012).
- ³⁹J. Kindervater, W. Haeusser, M. Janoschek, C. Pfleiderer, P. Boeni, and M. Garst, Phys. Rev. B **89**,180408 (2014).
- ⁴⁰E. Lelièvre-Berna, E. Bourgeat-Lami, S. Pujol, F. Thomas, X. Tonon, G. Pastrello, J. Alibon, B. Ouladiaff, L. Chapon, *Flipper 2013 Workshop*, ILL Grenoble (2013), p.122.
- ⁴¹P. G. Schmalen, Master thesis, TU München, Munich, Germany (2014).
- ⁴²V. Hutanu, Journal of large-scale research facilities **1**, A16 (2015).
- 43https://fzj.frm2.tum.de/